Biophysical Journal, Volume *111*

Supplemental Information

Polar Localization of the Serine Chemoreceptor of *Escherichia coli* Is Nucleoid Exclusion-Dependent

Ramakanth Neeli-Venkata, Sofia Startceva, Teppo Annila, and Andre S. Ribeiro

Supporting Material for "Polar Localization of the Serine Chemoreceptor of *Escherichia coli* is Nucleoid Exclusion-Dependent"

Ramakanth Neeli-Venkata, Sofia Startceva, Teppo Annila, and Andre S. Ribeiro

Fluorescent microplate reading

Aside from microscopy, the fluorescence from Tsr-Venus proteins under the control of P_{lac} was also measured with a Thermo Scientific* Fluoroskan Ascent Microplate Fluorometer. Cells of the SX4 strain at OD_{600} of ~0.3 were induced with various IPTG concentrations and grown at 37 °C with shaking, until reaching an OD_{600} ~ 0.6. From this, cells were centrifuged and suspended in PBS (Phosphate Buffered Saline). 150 µl of the cells that were suspended in PBS were taken and placed on a 96 well microplate and measured for relative fluorescence levels of Venus protein with excitation (509 nm) and emission (538 nm) wavelengths (1). We performed 3 independent experiments with 3 replicates per condition.

Image analysis

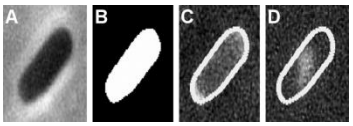

FIGURE S1 Example images used in Tsr clusters detection and nucleoid size and positioning estimation. (*A*) Phase contrast image. (*B*) Segmented cell by semi-automated segmentation from phase contrast image. (*C*) Corresponding fluorescent image for Tsr clusters detection (note the crescent shaped cluster at the lower pole) along with the detected cell border (segmented). (*D*) Example image of a cell with segmented border and fluorescence from a DAPI-stained nucleoid.

Stochastic models

Tsr is a trans-membrane protein that is not expected to be significantly affected by nucleoid exclusion when bound to the membrane. However, not all Tsr proteins are attached to the inner membrane at any given time. First, when produced, these proteins will diffuse in the cytoplasm, prior to reaching the inner membrane. Also, each Tsr is expected to be in a transient state between cytoplasmic and membrane-bound, with significant preference for the membrane-bound state. In particular, according to measurements (2), a significant fraction of Tsr proteins freely diffuse at any given moment, indicating that the rates of binding and unbinding of Tsr to the inner membrane likely do not differ by several orders of magnitude. We expect that it is when

unbound from the membrane that the Tsr proteins are subject to being excluded to the poles due to the presence of the nucleoid at midcell.

We implemented a 2-dimensional (2D) model, where the cell and nucleoid are modelled as rectangles with semicircular poles, as in previous models (2–7). Cell growth and nucleoid replication are not considered. The cell membranes and nucleoid are impenetrable to the Tsr clusters and, unless stated otherwise, the nucleoid center is precisely at the cell center (Fig. S2).

A model cell is a 2-dimensional grid of square blocks, with an inner and an outer membrane. The inner membrane is one-block-wide and encloses the intracellular environment. Tsr proteins can only enter a block of the inner membrane if Tol-Pal is present ('membrane blocks' with Tol-Pal are named 'Tol-Pal blocks'). The outer membrane is a 1-block-wide layer of blocks to which Tsr proteins cannot move to. Inner blocks occupied by the nucleoid or the cytoplasm are named 'nucleoid blocks' or 'cytoplasm blocks', respectively. Model Tsr proteins can move to any passable block at a fixed rate (nucleoid, inner membrane without Tol-Pal, and outer membrane blocks are not passable). At a Tol-Pal block, the rate of passage to a neighbor passable block is smaller than at a cytoplasm block.

The Tol-Pal diffusion-and-capture mechanism is implemented in the inner membrane blocks at the poles (Fig. S2), with each block having a rate of passage that is weighted so as to represent the 'binding strength' of Tol-Pal in a 3-dimensional cell. The concentration of Tol-Pal in a block decreases linearly with the distance from the block to the cell extremity, which allows modeling the gradual decrease of Tol-Pal with the distance from the cell extremities.

We implemented a 1-step stochastic model of expression of Tsr. Nevertheless, regarding where these proteins first appear in the cell, we account for the fact that the Tsr-Venus assembly process (namely, transcription, translation, folding, and chromophore maturation) takes 7.0 ± 2.5 min (1), with most of this time being spent in the last steps. This, combined with the fast diffusion rates when not in cluster formation (8), suggests that, by the time these proteins become active, they will be virtually randomly located in any of the cytoplasm or Tol-Pal blocks. As such, the location where they first appear is randomly selected. Finally, Tsr degradation is implemented by a zero order reaction whose rate is uniform in space. Unless stated otherwise, a simulation of each model cell is conducted for 2h prior to data acquisition (as model cells are initialized without Tsr proteins).

The aspect ratio of the cell and the nucleoid size (length and width) relative to the cell size were estimated from our empirical data. The length of the model cell, L, was set to 100 blocks, which we found to provide sufficient resolution. Fig. S1 depicts model cells with large (A, C) and small (B, D) nucleoids, as well as control (A, B) and deletion mutants for Tol-Pal (C, D).

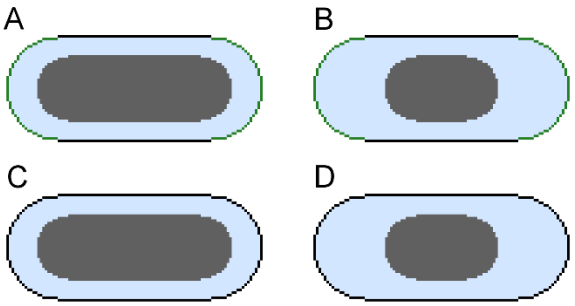

FIGURE S2. The blue area represents the cytoplasm, the grey area represents the nucleoid, the black lines represent membrane regions without Tol-Pal, and the green lines represent membrane regions with Tol-Pal (at the poles). In each model cell, the cell width is 0.42*L* and the nucleoid width is 0.26*L*. (*A*) control cell with relatively large nucleoid (0.76*L*), (*B*) Δ*tolpal* cell with relatively large nucleoid (0.76*L*), (*C*) control cell with relatively small nucleoid (0.44*L*), (*D*) Δ*tolpal* cell with relatively small nucleoid (0.44*L*). Only control cells have green lines.

Since our model is 2D, as mentioned above, we tuned the ability of each Tol-Pal block of capturing Tsr proteins as a function of its distance from the closest cell extremity, as this determines the number of Tol-Pal blocks that is expected to be at that distance in a three-dimensional (3D) model. For this, we:

1. Assume a 3D cell model, consisting of a cylinder of length 0.58*L* and radius 0.21*L* representing midcell and of two hemispheres of radius 0.21*L* each (representing the poles). Tol-Pal blocks are located along the cell inner membrane at the cell poles.

2. Split the cell into L slices along the major axis, each slice being 1 block wide.

3. Convert the 3D model into a 2D model, by setting in the 2D model, at each slice, the ability of Tol-Pal block(s) of capturing Tsr clusters as a function of the amount of Tol-Pal blocks in the corresponding slice in the 3D model (Table S1).

Supplementary Table S1 lists all reactions and events in model cells. The notation of the cell blocks is the following: c_{cyto} is a cytoplasm block, c_{TP} is a Tol-Pal block, $c_{passable}$ is a passable block (cytoplasm and Tol-Pal blocks), and $c_{neighbour}$ is an allowed destination for a moving Tsr protein (a passable block in the 4-neighbourhood of the block the protein is presently located in). A Tsr protein located in block c is denoted '$Tsr.c$'.

Reaction/event	Parameter	Description and references
$\varnothing \xrightarrow{k_{tsr}} Tsr.c_{passable}$	$k_{tsr} = \frac{1.4}{3 \cdot N_{passable}}$ sec^{-1}	Tsr production. The rate of Tsr production in each $c_{passable}$, is: $k_{tsr} = \frac{n_{burst}}{\tau_{mRNA} \cdot N_{passable}}$, with the average lifetime of mRNA, τ_{mRNA}, and the average number of Tsr proteins produced per burst, n_{burst}, being estimated from (1). $N_{passable}$ is the number of $c_{passable}$ blocks in the cell.
$Tsr.c_{passable} \xrightarrow{d_{tsr}} \varnothing$	$d_{tsr} = \frac{1}{1800}$ sec^{-1}	Tsr degradation reaction in each passable block (9).
$Tsr.c_{cyto} \xrightarrow{v_{cyto}} Tsr.c_{neighbour}$	$v_{cyto} = 1$ blocks/sec	Tsr motion reactions. Velocities v_{cyto} and v_{TP} were fit so that the spatial distributions of Tsr proteins for large and small nucleoids (after 2h of simulations) match the data from control cells. n_i is the number of Tol-Pal blocks in slice *i* of the 2D model, c_i is the circumference of the corresponding slice of the 3D model, ρ_i is the percentage of inner membrane blocks occupied with Tol-Pal, and r_i is the distance (in blocks) from the slice *i* to the cell extremity along the major cell axis. When $r_i = 0.21L$, Tol-Pal is removed from the inner membrane block.
$Tsr.c_{TP} \xrightarrow{\alpha_i \cdot v_{TP}} Tsr.c_{neighbour}$	$v_{TP} = 1$ blocks/sec $\alpha_i = \frac{n_i}{c_i \cdot \rho_i}$ $\rho_i = \frac{0.21L - r_i}{0.21L}$ $i \in [1, L]$	

TABLE S1: Reactions, parameters, and events in model cells.

Results

Expression of Tsr-Venus as a function of induction strength

We measured Tsr-Venus expression as a function of induction strength with a microplate fluorometer at 37 °C (Fig. S3 *A*). A fold change of ~110 was observed when increasing IPTG levels from 0 to 1000 μM ml^{-1}, in agreement with a previous study (1).

Next, by live cell microscopy, with cells kept at 37 °C prior and during observation, we measured the fluorescence intensity of Tsr-Venus from individual cells (Methods) when increasing IPTG levels from 0 to 500 μM ml^{-1}, 2 hours after induction of the target gene. The mean Tsr-Venus levels detected from the images show close agreement with the microplate fluorometer measurements (Fig. S3 *B*). We conclude that the quantification methods of Tsr-Venus levels from live cell imaging are accurate.

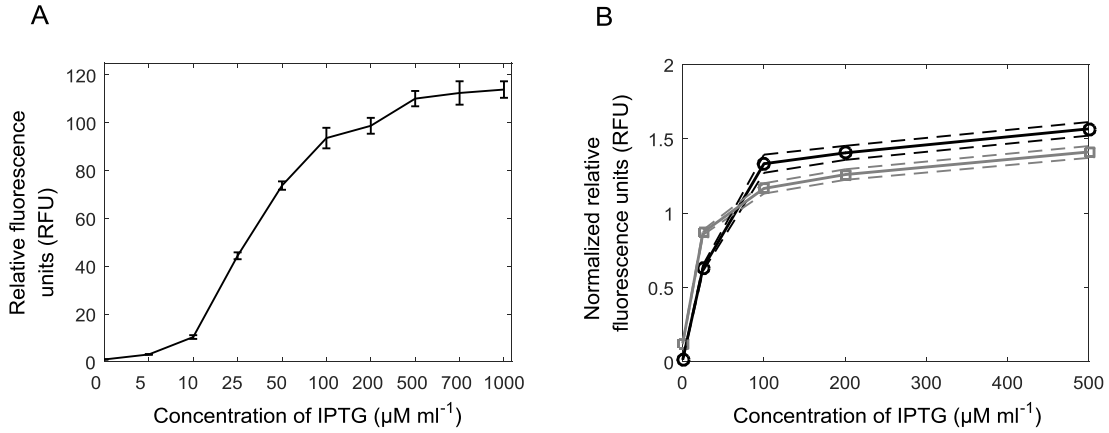

FIGURE S3. Induction curves of Tsr-Venus. (*A*) Mean expression levels of the target proteins (Tsr-Venus) estimated by microplate fluorometer as a function of the induction level by IPTG. Error bars are the standard deviation of three independent measurements. (*B*) Comparison of the induction curves (normalized by the mean, in arbitrary units) when measured by microplate fluorometer (black line) and by confocal microscopy (grey line), from live cells, 2 hours after induction by IPTG, for varying IPTG concentrations. Only the conditions observed in both the microscope and the plate reader are shown. Dashed lines are the standard deviation of the relative fluorescence units (RFU) from independent measurements, at each IPTG concentration.

Ampicillin treated cells

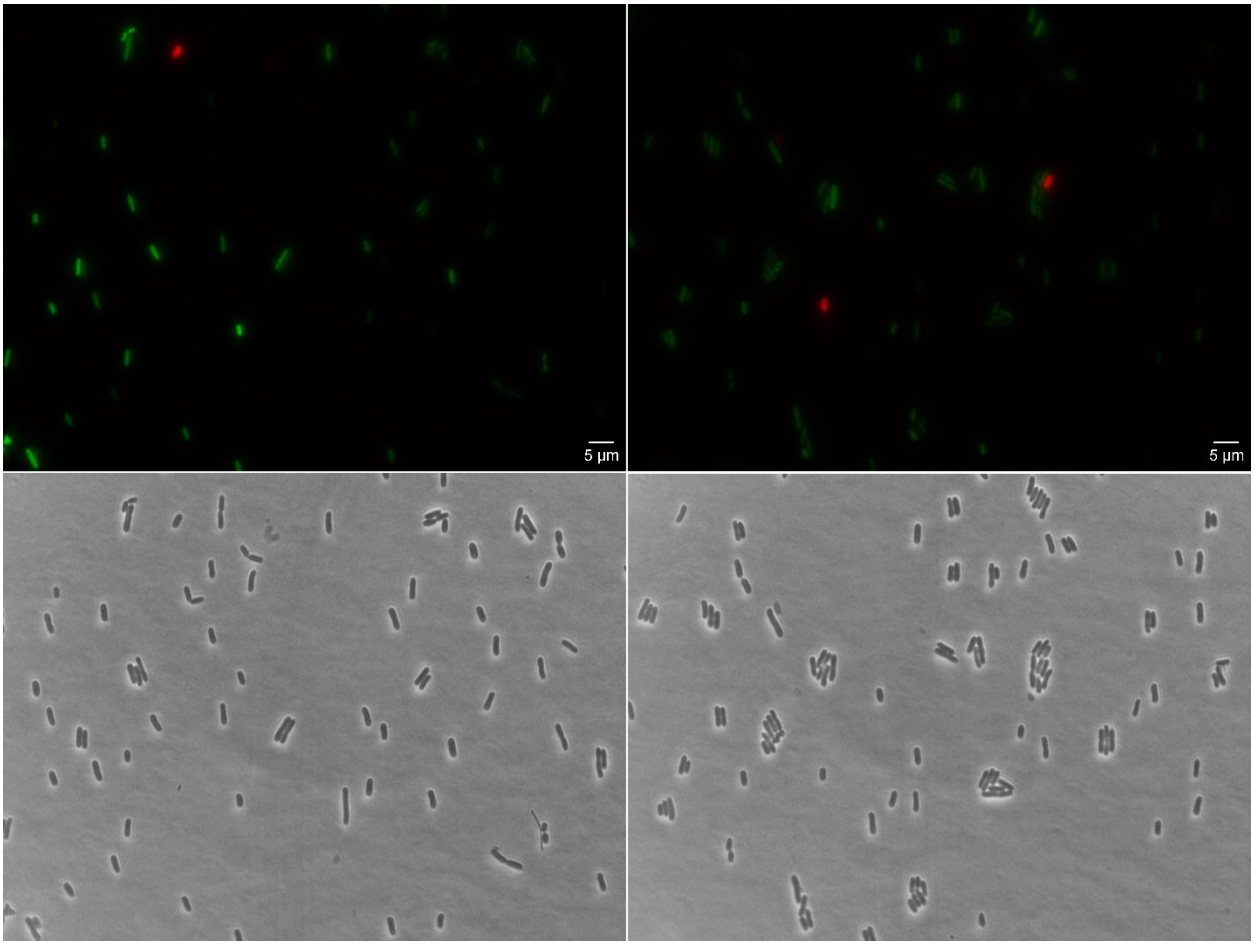

FIGURE S4. Epifluorescence microscopy images of cells treated with ampicillin (top right) and control cells (top left) subject to a BAC Live/Dead Assay. Green is indicative of viability while red is indicative of death cells. Visibly, the population subject to ampicillin contains several viable cells that were used for further analysis. In these experiments, expression of Tsr-Venus is not activated, so as to not generate 'background' fluorescence. Also shown are phase contrast images of the cells treated with ampicillin (bottom right) and control cells (bottom left).

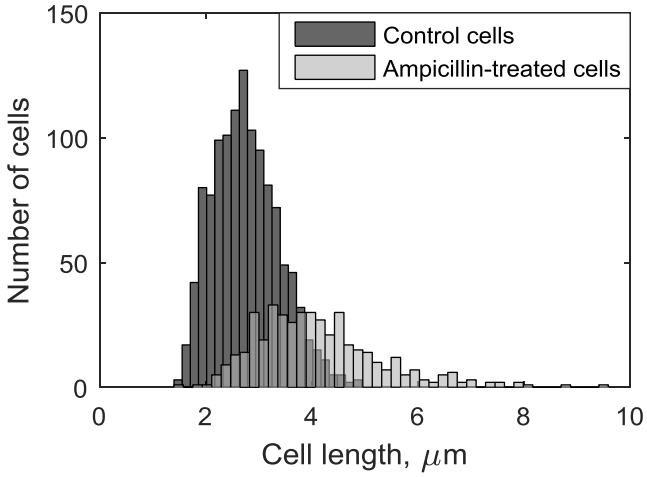

FIGURE S5. Distribution of individual cell length from 436 cells treated with ampicillin (light grey) and from 1195 control cells (dark grey). In these experiments, expression of Tsr-Venus is activated.

Degree of symmetry of the process of segregation of Tsr clusters to the poles

We quantified the degree of symmetry of the process of segregation of Tsr clusters to the poles, relative to the poles age. For this, based on data obtained from time-lapse microscopy measurements (Methods), from the fluorescence along the major cell axis of individual cells and the definition of poles and midcell (main manuscript), we determined the fraction of cells with higher fluorescence intensity at the old pole compared to the new pole, the moment prior to dividing. Then, we tested whether the measured biases could arise from sampling from an unbiased binomial distribution.

For this test, we analyzed SX4 cells (216 cells), kept at 37 ºC prior and during observation. We observed that 63% of the cells contained more Tsr at the old pole (*p*-value of 0.6×10^{-5} from a binomial test that the measured distribution can be distinguished from an unbiased binomial distribution), in agreement with previous studies (10).

This statistically significant bias could result from the presence of inherited clusters (which locate solely at old poles), rather than the process of segregation to the poles (11). To assess this, to the distribution of fluorescence along the major cell axis of each cell prior to its division, we discounted the same distribution obtained when the cell was born. As such, we obtained an approximate distribution of fluorescence of proteins produced during the cells' lifetime. From these (216 cells), we obtained the numbers of cells with larger and smaller amounts of Tsr-Venus at the old pole. Next, we calculated the same p-value as before, by comparing the empirical distribution with an unbiased binomial distribution. This *p*-value is larger than 0.05, from which

we conclude that the process of segregation of Tsr clusters to the poles is symmetric relative to the poles age (as reported in (10)).

From these measurements it is also possible to conclude that cell divisions introduce non-negligible biases in the numbers of Tsr-Venus between old and new poles of the cells, in agreement with (10).

Tsr clusters location when first detected

We studied, from time-lapse microscopy data, the location of Tsr clusters when first detected in control cells where the induction of Tsr-Venus was made while the cells were already under observation. From Fig. S6, most clusters are already at the poles when first observed.

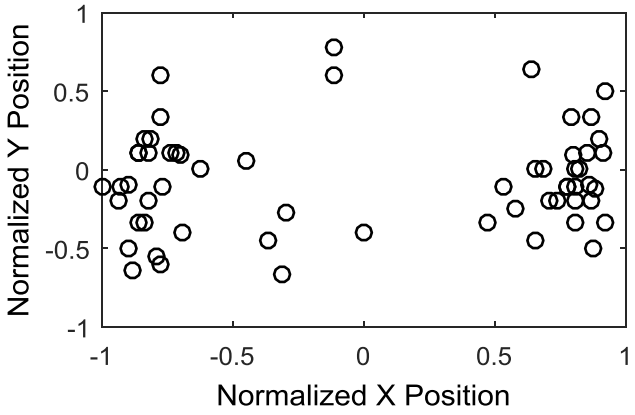

FIGURE S6. Relative positioning of Tsr-Venus clusters when first detected during a cell's lifetime (X and Y axes normalized to the interval [-1, 1]). We arbitrarily set the 'left pole' and 'top of the cell' as the negative (-1) and the 'right pole' and 'bottom of the cell' as positive (+1), with 'left', 'right', 'top' and 'bottom' being defined by the positioning of the cell in the image.

Tsr clusters location as a function of relative nucleoid length

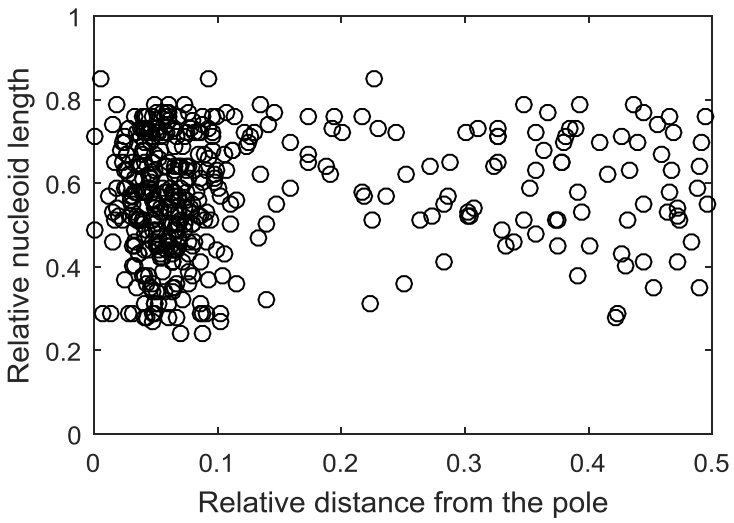

FIGURE S7: Relative nucleoid length versus relative distance of individual Tsr clusters from the closest cell extremity in WT cells.

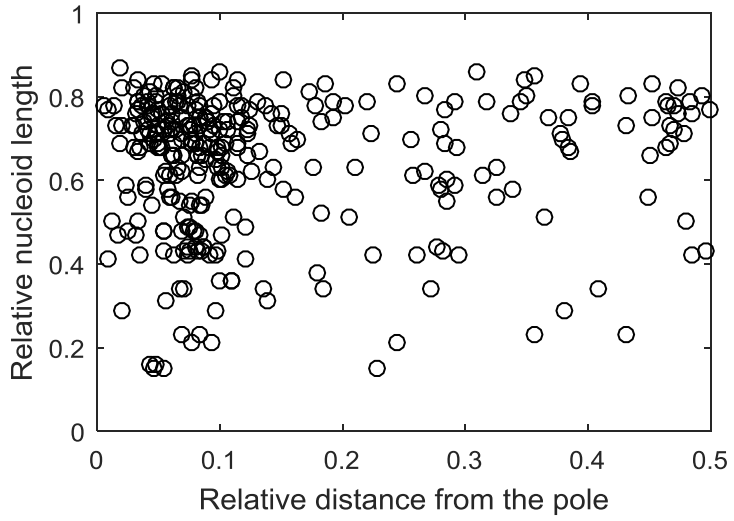

FIGURE S8: Relative nucleoid length versus relative distance of individual Tsr clusters from the closest cell extremity in Δ*tolpal* cells.

Comparison of DAPI staining and HupA-mCherry tagging

As noted in the main manuscript, Tsr-Venus distributions are identical in cells stained with DAPI and cells expressing HupA-mCherry at 37 °C (Fig. S9). As expected, they are also identically anti-correlated with the distributions of nucleoid(s) fluorescence (Pearson correlation equaled -0.87). Finally, the p-value of the *t*-test of statistical significance assuming that the data are uncorrelated was smaller than 10^{-4}, i.e. the anti-correlation is statistically significant.

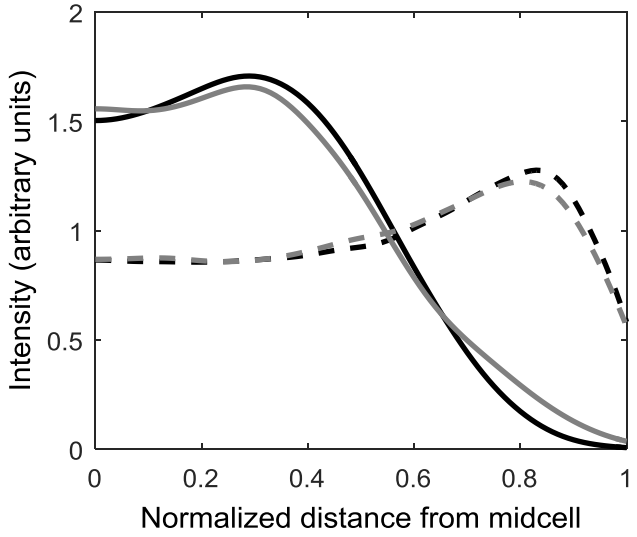

FIGURE S9. Kernel density estimates (KDEs) of the spatial distributions of the background-subtracted fluorescence of cells with the nucleoids stained by DAPI (black lines, 125 cells) and by HupA-mCherry (grey lines, 58 cells). Also shown (dashed lines) are the KDEs of fluorescence intensities (arbitrary units) of Tsr-Venus along the major cell axis (bandwidths 0.05) of the same cells.

Correlations between Tsr clusters spatial distributions as estimated from the empirical data

Strain, Nucleoid length	**WT, large**	**WT, small**	**Δ*tolpal*, large**
Δ*tolpal*, small	$p = 0.05$	$p = 0.17$	$p = 0.75$
Δ*tolpal*, large	$p < 0.01$ $r = 0.75$ $r \in [0.33, 0.92]$	$p < 0.01$ $r = 0.69$ $r \in [0.21, 0.90]$	
WT, small	$p < 0.01$ $r = 0.61$ $r \in [0.08, 0.87]$		

TABLE S2 *p*-values of the Pearson correlation between Tsr clusters spatial distributions in WT and Δ*tolpal* cells with relatively large (occupying ≥ 65% of the cell length) and small (occupying ≤ 35% of the cell length) nucleoids. When the correlation is significant ($p < 0.01$), the Pearson correlation value *r*, and the 95% CI of *r* are also shown.

Correlations between Tsr clusters spatial distributions in the stochastic models of nucleoid exclusion of Tsr clusters from midcell

Strain, **Nucleoid length**	**WT,** **large**	**WT,** **small**	**Δ*tolpal*,** **large**
Δ*tolpal*, **small**	$p = 0.19$	$p < 0.01$ $r = 0.52$ $r \in [0.29, 0.70]$	$p < 0.01$ $r = 0.44$ $r \in [0.18, 0.64]$
Δ*tolpal*, **large**	$p \ll 0.01$ $r = 0.82$ $r \in [0.71, 0.90]$	$p \ll 0.01$ $r = 0.80$ $r \in [0.67, 0.88]$	
WT, **small**	$p \ll 0.01$ $r = 0.93$ $r \in [0.87, 0.96]$		

TABLE S3 *In silico* model. *P*-values of the Pearson correlation between Tsr clusters spatial distributions in WT and Δ*tolpal* cells with relatively large and small nucleoids. When the correlation is significant ($p < 0.05$), the Pearson correlation value *r*, and the 95% CI of *r* are also shown. The data from each condition is from 1000 cells.

SUPPORTING REFERENCES

1. Yu, J., J. Xiao, X. Ren, K. Lao, and X.S. Xie. 2006. Probing gene expression in live cells, one protein molecule at a time. Science. 311: 1600–3.
2. Oh, D., Y. Yu, H. Lee, B.L. Wanner, and K. Ritchie. 2014. Dynamics of the serine chemoreceptor in the escherichia coli inner membrane: A high-speed single-molecule tracking study. Biophys. J. 106: 145–153.
3. Koch, A.L., and J. V. Holtje. 1995. A physical basis for the precise location of the division site of rod-shaped bacteria: The Central Stress Model. Microbiology. 141: 3171–3180.
4. Helgesen, E., S. Fossum-Raunehaug, and K. Skarstad. 2016. Lack of the H-NS protein results in extended and aberrantly positioned DNA during chromosome replication and segregation in Escherichia coli. J. Bacteriol. 198: 1305–1316.
5. Fisher, J.K., A. Bourniquel, G. Witz, B. Weiner, M. Prentiss, and N. Kleckner. 2013. Four-Dimensional Imaging of E . coli Nucleoid Organization and Dynamics in Living Cells. Cell. 153: 882–895.
6. Zimmerman, S.B. 2006. Shape and compaction of Escherichia coli nucleoids. J. Struct. Biol. 156: 255–61.
7. Fritsche, M., S. Li, D.W. Heermann, and P.A. Wiggins. 2012. A model for Escherichia coli chromosome packaging supports transcription factor-induced DNA domain formation. Nucleic Acids Res. 40: 972–980.
8. Elowitz, M.B., M.G. Surette, P. Wolf, J.B. Stock, and S. Leibler. 1999. Protein Mobility in the Cytoplasm of. 181: 197–203.
9. Taniguchi, Y., P.J. Choi, G.W. Li, H. Chen, M. Babu, J. Hearn, A. Emili, and X.S. Xie. 2010. Quantifying E. coli Proteome and Transcriptome with Single-Molecule Sensitivity in Single Cells. Sci. (New York, NY). 329: 533–538.
10. Ping, L., B. Weiner, and N. Kleckner. 2008. Tsr-GFP accumulates linearly with time at cell poles, and can be used to differentiate “old” versus “new” poles, in Escherichia coli. Mol. Microbiol. 69: 1427–38.
11. Gupta, A., J. Lloyd-Price, R. Neeli-Venkata, S.M.D. Oliveira, and A.S. Ribeiro. 2014. In vivo kinetics of segregation and polar retention of MS2-GFP-RNA complexes in Escherichia coli. Biophys. J. 106: 1928–37.